(Received 17 October 2025, Accepted 25 December 2025, Scheduled 30 January 2026)

A Double Crescent Slots Circular Ultra-Wideband Monopole Antenna for 5G, MBAN/WBAN and Future Internet of Things Applications

Djamel Sayad[1], Rami Zegadi[2], Nor-elhouda Mehenni[2], Issa Elfergani[3,4], Sarra Khacha[2], Mohamed L. Bouknia[2], Almudena Rivadeneyra[5], Atul Varshne[6], Jonathan Rodriguez[3], and Chemseddine Zebiri[1,*]

[1]*Laboratoire d'Electronique de Skikda (LRES), Department of Electrical Engineering University 20 Aout 1955-Skikda, 21000 Skikda, Algeria*
[2]*Laboratoire d'Electronique de Puissance et Commande Industrielle (LEPCI) Department of Electronics, University of Ferhat Abbas, Setif-1, Setif 19000, Algeria*
[3]*Instituto de Telecomunicações, Campus Universitário de Santiago, 3810-193, Aveiro, Portugal*
[4]*Faculty of Engineering and Informatics, University of Bradford, Bradford, UK*
[5]*Engineering Group for Power Electronics and Instrumentation (ELI), Faculty of Sciences Department of Electronics and Computer Technology, University of Granada, Spain*
[6]*Electronics and Communication Engineering Department, FET Gurukula Kangri (Deemed to be University), Haridwar, Uttarakhand 249404, India*

ABSTRACT: This paper presents the design, optimization, and experimental validation of a compact ultra-wideband (UWB) circular monopole antenna achieving a 3.05–23.04 GHz impedance bandwidth on a low-cost FR4 substrate ($\epsilon_r = 4.4$, 0.8 mm thick, $30 \times 20\,\text{mm}^2$). The structure incorporates dual crescent-shaped slots and a defected ground structure (DGS) to enhance bandwidth and gain. The antenna was designed and optimized using ANSYS HFSS. Parametric optimization through four design steps demonstrated the impact of feed offset, slot incorporation, and ground-plane modification on impedance matching. The measured $S_{11} < -10$ dB covered a UWB, spanning the sub-6 GHz, C, X, Ku, and K bands, with radiation efficiency of about 86% across the band. The antenna exhibited a peak gain of up to 6.6 dBi with nearly omnidirectional radiation at lower frequencies and more directive patterns at higher bands. Simulated and measured results validated the wideband performance and high radiation efficiency, and they agree within ± 2 dB in gain in the band up to 18 GHz. The design enables cost-effective deployment in high-speed wireless data transmission, 5G, IoT, radar, and biomedical imaging applications.

1. INTRODUCTION

Ultra-wideband (UWB) technology has become one of the most attractive solutions for high-capacity and short-range wireless communication since the Federal Communications Commission (FCC) allocated the frequency range of 3.1–10.6 GHz for unlicensed use in 2002. Planar UWB monopole antennas are pivotal in communication and imaging systems requiring a wide bandwidth and easy integration. Operating within the FCC-defined UWB range of 3.1–10.6 GHz, these compact radiators leverage innovative geometries such as slots, fractal patterns, and multiport networks to achieve additional resonances and targeted notches without significantly increasing their size [1]. For example, a planar monopole with a ribbon-shaped slot operates from 3.1 to 10.8 GHz on an FR_4 substrate, demonstrating the effectiveness of slotted designs in achieving wide bandwidth within a compact form [2]. This concept is further advanced through a circular octagonal slot configuration, providing multi-resonant performance and enhanced compactness for UWB applications [3]. In [4, 5], the presented monopole antennas preserve UWB operation while using SRR cells and L-shaped slits, respectively, to introduce precise band rejection characteristics. This frequency range supports high-speed wireless networks and miniature radar systems, with advanced designs extending to higher frequencies [6, 7]. Microstrip patch antennas, particularly compact and versatile designs, are critical for modern communication systems, such as 5G and radar/internet of things (IoT) applications. Circular patch antennas with slots offer a low profile, easy integration, and multi-resonant capabilities, making them ideal for sub-6 GHz to mmWave bands [8]. The strategic placement of slots or coupling elements on the radiator or ground plane enables multi-band responses [9]. In UWB microstrip antennas, the radiator geometry and defected ground structures (DGSs) control the current distribution, input impedance, and rejection or folded bands [10–12]. Combining patch geometries with a DGS expands the bandwidth and introduces specific notches [13, 14]. Common patch shapes are rectangular, circular, annular, elliptical, crescent, triangular, fractal, and polygonal, and they interact with DGS patterns

* Corresponding author: Chemseddine Zebiri(czebir@univ-setif.dz).

to achieve targeted UWB performance [10, 11, 13, 15, 16]. Circular, annular, and octagonal patches are favored for their simple mode arrangement, often paired with modified ground elements or DGS for notches or specific bands [11, 16–18]. Elliptical patches provide geometric flexibility for tailoring impedance and current distribution, using slots or folding elements for targeted notches [16, 19–22]. Crescent-shaped patches and curved designs introduce asymmetry in mode control and slot integration, enabling notches in specific spectral positions, often with conical or tailored microstrip feedlines for compact medical or biomedical applications [23, 24]. Polygonal (e.g., pentagonal, hexagonal) and fractal patches with internal patterns such as fractal or Sierpinski slots generate multiple spectral peaks or enhanced notches, leading to an extended bandwidth [25, 26]. Designers achieve wider bands and multi-band functionality using radiator slots (e.g., crescent, U-shaped, elliptical), surface-loading techniques such as frequency selective surfaces, electromagnetic band-gap (EBG) or split ring resonator structures, and coplanar waveguide (CPW) or microstrip feeds to enhance gain and isolation while maintaining a broad bandwidth [27–30]. A compact UWB monopole with a ribbon-shaped slot demonstrates an ultra-wide impedance bandwidth and near-omnidirectional radiation suitable for indoor environments [31], whereas a slotted circular patch configuration effectively controls resonant modes to achieve broad bandwidth and stable monopole radiation characteristics [32]. Optimized DGS configurations (e.g., rectangular, Pi/T-slots) adjust impedance, widen bandwidth, or create notch resonances, with studies offering benchmarks for return loss and ground ergonomics[13, 14, 33]. Reduced ground planes with DGS and tailored radiators maintain gain and isolation while minimizing size, which is crucial for portable and biomedical devices [10, 12–14, 33–36]. UWB antennas support applications in biomedical imaging (e.g., breast or kidney cancer detection) [37, 38], wireless body area networks (WBANs), IoT systems [39], geophysical detection (GPR) [40], automotive networks, and Wi-Fi/WLAN with reconfigurable notches [7, 41–45]. Practical trends involve substrates such as FR-4, kappa, or flexible materials, along with integration solutions such as baluns, adaptable notches, and metamaterials, enabling miniaturized UWB designs for 3–24 GHz systems in MBAN/WBAN and IoT applications [5, 46]. The demand for compact, wide-bandwidth, and multi-resonant antennas for 5G and IoT drives UWB and planar monopole designs, offering simple integration and low profiles for mobile and IoT devices [47–49]. The recent research on UWB printed monopole antennas has focused primarily on achieving broad impedance bandwidths while maintaining the inherent advantages of this class of antennas [30, 49]. However, many reported structures still suffer from limited bandwidth extension, particularly toward the lower edge, owing to profile constraints and performance degradation at higher frequencies due to substrate limitations. In this context, there remains a need for simple antenna geometries capable of covering not only the classical UWB range but also the upper microwave region beyond 10.6 GHz for emerging wideband applications. In this study, we develop a compact printed monopole antenna in a progressive, step-by-step manner, where each geometric modification contributes to bandwidth enhancement. Although the initial aim of this work was to develop a compact UWB monopole antenna that covers the conventional FCC UWB, the stepwise optimization techniques have led to a much broader operating range extending up to 23 GHz. This result is particularly relevant given the growing interest in wide-band and multi-band wireless systems. However, the implementation of such extended UWB designs on low-cost FR4 substrates poses a serious challenge. FR4 is known to exhibit increased dielectric loss, dispersion, and reduced stability above approximately 12 GHz, which can affect both the impedance matching and the radiation efficiency of the prototype. The research on UWB printed monopole antennas has increasingly focused on achieving extremely wide impedance bandwidths while maintaining their inherent advantages, such as simple geometry, low cost, and ease of fabrication. Although FR4 is traditionally considered unsuitable for millimeter-wave applications owing to its dielectric losses, it continues to be widely used in antenna applications owing to its affordability, fabrication simplicity, and acceptable performance when being properly optimized. Several studies have demonstrated that FR4-based antennas can operate at frequencies above 12 GHz. A compact triple-band antenna on FR4 operating up to 14 GHz with good impedance matching and an efficiency reaching 87% was reported in [24]. A broadband FR4-based antenna for 5G mmWave applications was designed in [50]. The design operates in the 23–29 GHz range, achieving a 5 dBi gain. A low-profile, high-efficiency (87%), 28 GHz microstrip antenna with SIW integration on FR4 was developed in [31]. Similarly, a UWB FR4 design is presented in [51], covering 3.2–23.9 GHz while maintaining stable radiation patterns and a peak gain of 6.2 dB.

This paper proposes a compact circular patch antenna with dual crescent slots, operating from 3 to 24 GHz, tailored for sub-6 GHz and partially millimeter-wave 5G and radar/IoT applications. By introducing crescent slots, the design achieves multiple resonances and UWB without compromising the low profile or ease of integration. Crescent slots have been proven for multi-band or wide-band responses in compact wireless systems [52, 53] with slot geometry critical for 5G applications [54]. Recent studies have highlighted crescent slots for WLAN and ISM bands, showing enhanced bandwidth antenna designs [55–57]. The proposed dual-crescent-slot circular monopole antenna targets UWB (3–24 GHz) performance for future 5G and IoT applications, building on findings that crescent slots enable multi-band responses [48, 58, 59]. The design emphasizes compactness, wide impedance bandwidth, and efficient radiation, while avoiding overly complex geometries or auxiliary structures. Compared with existing UWB antennas, the proposed antenna achieves a broader operating range and higher versatility, positioning it as a promising candidate for future high-data-rate and multi-standard communication systems.

2. PROPOSED ANTENNA DESIGN

The proposed antenna is a compact printed monopole designed on an FR4 substrate ($\epsilon_r = 4.4$) with overall dimensions of $30 \times 20 \times 0.8\,\text{mm}^3$ (Figure 1). The top surface comprises a cir-

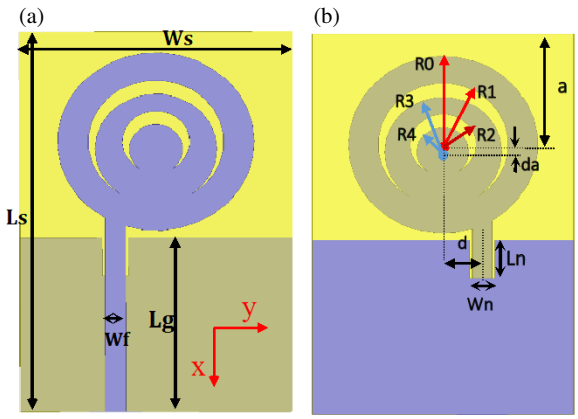

FIGURE 1. Proposed UWB slotted circular shaped monopole antenna. (a) Top and (b) bottom view.

cular radiating patch with radius R_0= 7.25 mm, modified with two concentric crescent-shaped slots and excited by a 50 Ω microstrip feed line offset from the patch center. A partial ground plane was implemented on the bottom surface by incorporating a rectangular notch to achieve proper impedance matching and enhance the frequency bandwidth.

The combination of a circular patch with crescent-shaped slots, offset feeding, and a defected ground structure enables the antenna to excite multiple resonant modes, achieving ultra-wideband functionality in a compact form suitable for modern wireless applications. The antenna dimensions were optimized to ensure proper impedance matching and stable omnidirectional radiation across the entire UWB spectrum. Table 1 summarizes the optimized geometrical parameters of the proposed antenna. The optimized design ensures high performance and makes the antenna suitable for modern wireless communications.

TABLE 1. Optimized geometrical parameters of the proposed antenna.

Parameter	Value (mm)	Parameter	Value (mm)
L_s	31	R_3	4.5
W_s	20	R_4	2
L_g	14.2	a	9
W_f	1.5	d_a	0.5
R_0	7.25	L_n	3.1
R_1	5	W_n	1.9
R_2	2.5	d	3

3. ANTENNA DESIGN STEPS

The proposed monopole antenna was developed through four iterative design steps, as illustrated in Figure 2, with the corresponding intermediate reflection coefficient responses shown in Figure 6 and peak gain results in Figure 7. The initial configuration consists of a simple, regularly shaped circular monopole with a center-fed microstrip line. This basic design exhibits a triple-band response covering 3.33–10.27 GHz, 13.64–23.04 GHz, and 24.54–29.28 GHz bands, for various multi-band wireless and radar applications (Figure 3(a)). In Step 2, the excitation line is shifted from the center, leading to a significant enhancement of the first band, which expands to 3.36–13.64 GHz. This improvement occurs at the expense of the second band, which narrows to 19.49–22.32 GHz, whereas the third band remains almost unchanged (24.95–28.78 GHz) (Figure 3(b)). This shift demonstrates the sensitivity of the impedance matching and resonance behavior to feed position, enabling better control of the antenna's frequency response.

In Step 3a, the introduction of two crescent-shaped slots improves impedance matching, particularly at low frequencies. As a result, the first operating band extends by approximately 250 MHz, covering 3.11–13.54 GHz, while the second and third bands remain nearly unchanged compared to Step 2. This modification provides broader low-frequency coverage and ensures stable behavior across the higher bands without increasing the overall size of the antenna. Step 3b is included to isolate and highlight the specific influence of the crescent slots on the antenna's frequency response, mainly in the lower band. Without the slots, even with the ground-plane notch, the lower cutoff cannot be pushed below 3.32 GHz (Figure 3(c)), indicating that the slots play a central role in extending the first band. Finally, in Step 4, combining both the crescent slots and the ground-plane notch complements their individual effects, improving mode excitation and effectively merging the first two bands. This combined mechanism lowers the overall cutoff to 3.05 GHz and enables a UWB response spanning 3.05–23.04 GHz, along with a secondary band at 24.54–29.28 GHz (Figure 3(d)). The final configuration offers seamless broadband operation with a compact geometry and a simplified structure. In Step 3, the introduction of two crescent-shaped slots further enhances the impedance matching and radiation performance. As a result, the first operating band extends by approximately 250 MHz, covering 3.11–13.54 GHz, whereas the second and third bands remain nearly unchanged compared to Step 2. This modification provides broader low-frequency coverage and ensures stable behavior across higher bands without increasing the overall antenna size. The optimized design is well-suited for a variety of modern applications, including high-speed wireless data transmission (WPAN, WLAN), indoor localization and sensing, biomedical monitoring, non-cooperative radar imaging, and 5G mmWave communication systems, as well as supporting standards such as Wi-Fi, LTE, GPS, and UWB sensing technologies. Table 2 summarizes the antenna evolution steps with the corresponding operating frequency bands and related applications.

3.1. Parametric Study

This section presents the parametric analysis conducted to evaluate the influence of key geometrical parameters on the antenna performance. The study begins by introducing a single crescent-shaped slot defined by R_1 and R_3. This slot has a clear impact on impedance matching, shifting the lower edge of the operating band by approximately 200 MHz compared with the slotless configuration as shown in Figure 4. For instance, when $R_1 = 5$ mm and $R_3 = 4.5$ mm, the antenna becomes matched from 3.25 GHz, whereas the slotless structure starts at 3.45 GHz. For $R_1 = 6$ mm and $R_3 = 1.5$ mm, the lower edge can be pushed down to 3.18 GHz, although some mismatch ap-

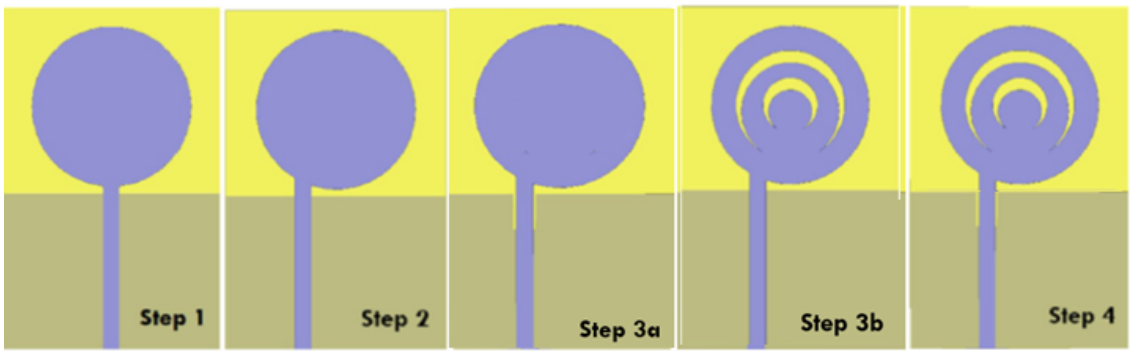

FIGURE 2. Design evolution of the proposed circular shaped monopole antenna.

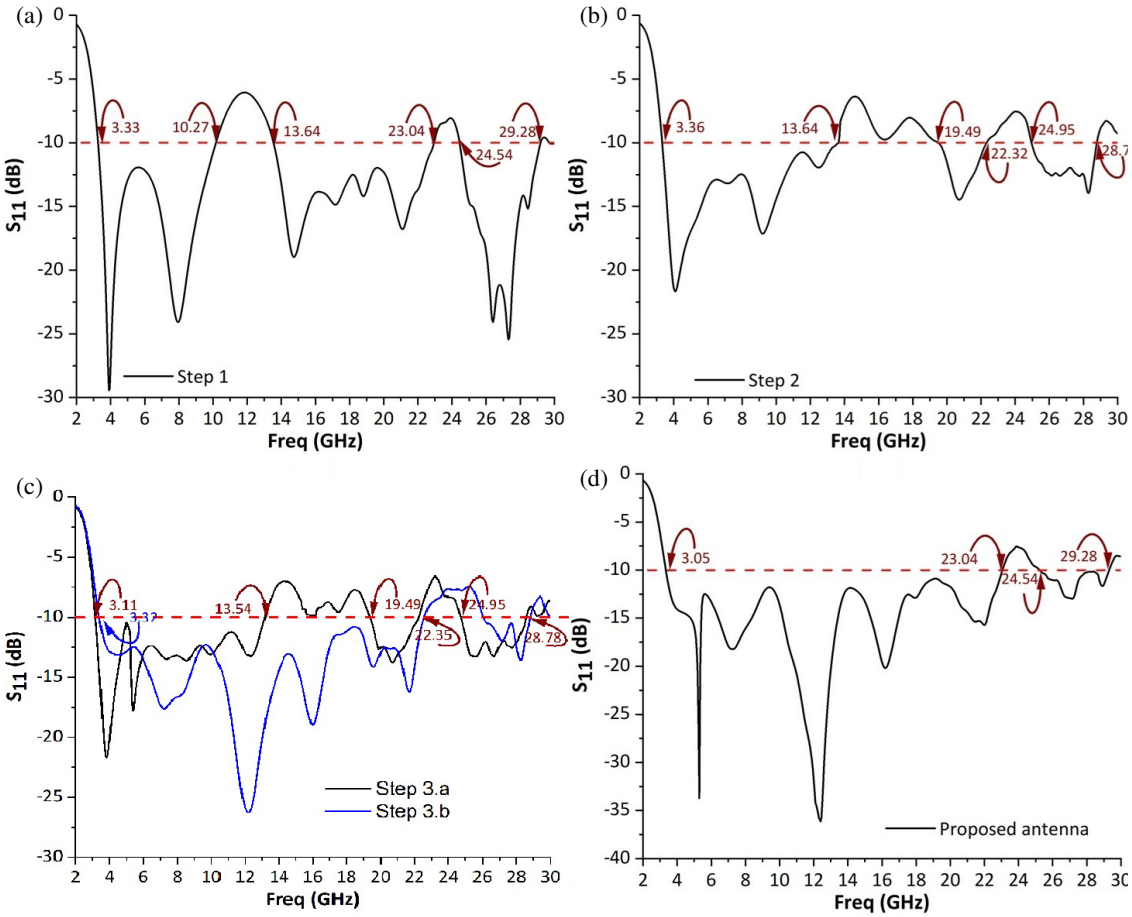

FIGURE 3. S_{11} of different design steps of the proposed monopole antenna (design evolution steps). (a) Step 1, (b) Step 2, (c) Step 3, and (d) Step 4 (final proposed structure).

pears around 9–10 GHz. Introducing a second crescent slot, defined by R_2 and R_4, further shifts the first resonance downward by approximately 100 MHz, for $R_2 = 2.5$ mm and $R_4 = 2$ mm (Figure 5). This behavior can be attributed to the presence of an additional equivalent LC resonator that lowers the fundamental resonance frequency. At higher frequencies, this second slot becomes electrically significant (its physical length approaches the wavelength λ), thus exerting a stronger influence on the antenna response. The last phase of the parametric study examined the effects of the ground-plane notch. The ground plane notch improves impedance matching and enhances the high-frequency bandwidth in planar antennas [23, 36, 60–62]. A rectangular ground plane notch ($L_n \times W_n$) was introduced, leading to the final antenna configuration. The parametric results confirm that the ground plane notch plays a key role in improving the impedance matching by bringing multiple resonant modes closer together. As shown in Figure 6, this modification, for $L_n = 3.1$ mm and $W_n = 1.9$ mm, enables a wide and continuous bandwidth with $S_{11} \leq -10$ dB from 3.05 GHz to 24 GHz, effectively covering several key services, including UWB, Ku-band satellite communications (12–18 GHz), lower

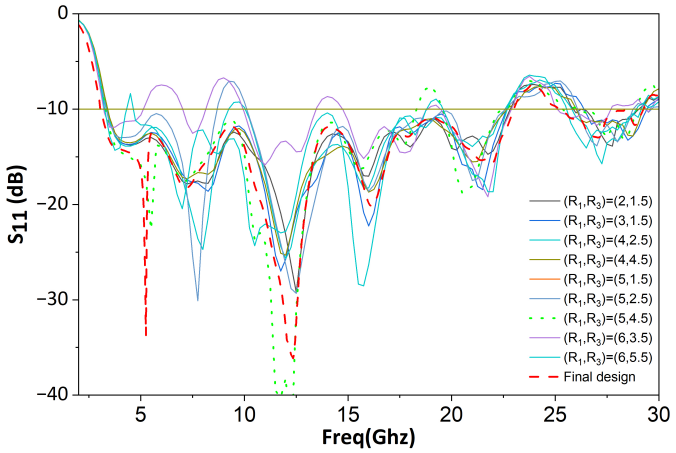

FIGURE 4. Effect of the first crescent-shaped slot on the reflection coefficient (S_{11}) of the proposed antenna.

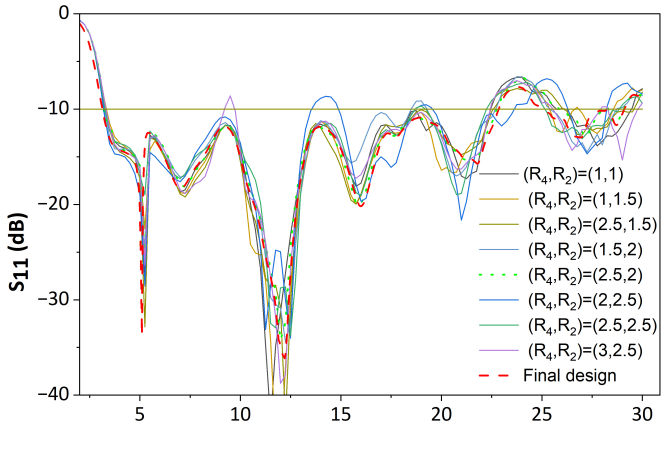

FIGURE 5. Effect of the second crescent slot on the reflection coefficient (S_{11}) and bandwidth enhancement.

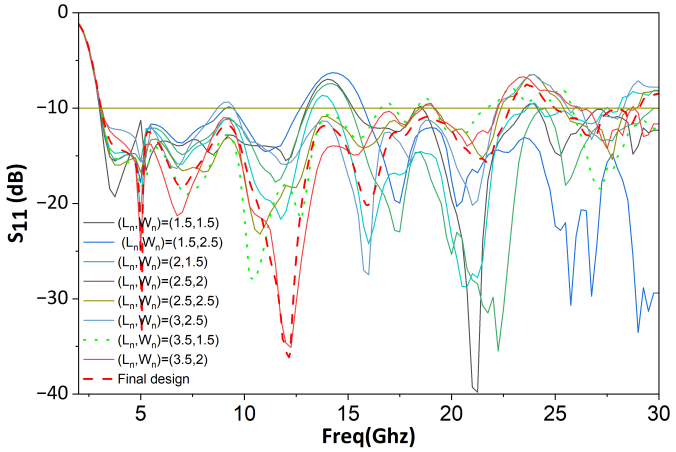

FIGURE 6. Effect of the ground-plane notch on impedance matching (S_{11}) and final bandwidth extension of the optimized antenna design.

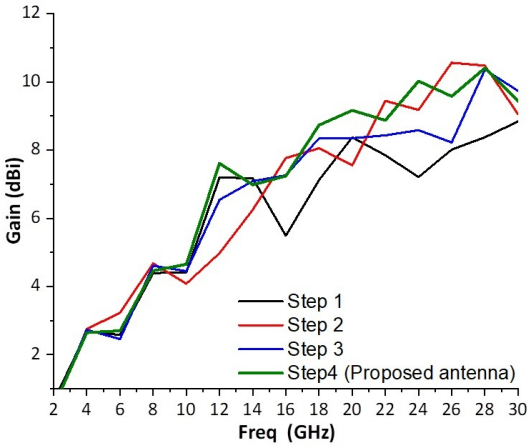

FIGURE 7. Gain of different design steps of the proposed monopole antenna.

TABLE 2. Antenna evolution steps, operating frequency bands and related applications.

Design Step	Configuration Description	Operating Freq. Bands (GHz)	Characteristics/Applications
Step 1	Basic circular monopole with center-fed line	3.33–-10.27, 13.64–-23.04, 24.54–-29.28	Triple-band operation; suitable for multi-band wireless, radar, and satellite links
Step 2	Feed line shifted from center	3.36–-13.64, 19.49–-22.32, 24.95–-28.78	Extended low-frequency bandwidth; improved impedance matching; applications in WLAN and broadband communication
Step 3	Introduction of two crescent shaped slots	3.11–-13.54, 19.49–-22.32, 24.95–-28.78	Further bandwidth enhancement; supports WiMAX, LTE, and sensing systems
Step 4	Ground plane with notch for impedance adaptation	3.05–-23.04, 24.54–-29.28	UWB coverage; supports 5G *mmWave*, UWB radar, biomedical, and *IoT* applications

K-band (18–21 GHz), and emerging 5G/pre-6G mm-wave allocations around 22–23.6 GHz.

The peak gain plots for the four antenna design steps (Figure 7) demonstrate that the Step 4 design achieves consistent improvements over the prior steps across the 10–30 GHz frequency band, with enhanced performance in terms of higher gain values and a better overall efficiency. However, in the specific bands of 4–8 GHz and 25–28 GHz, the Step 2 design

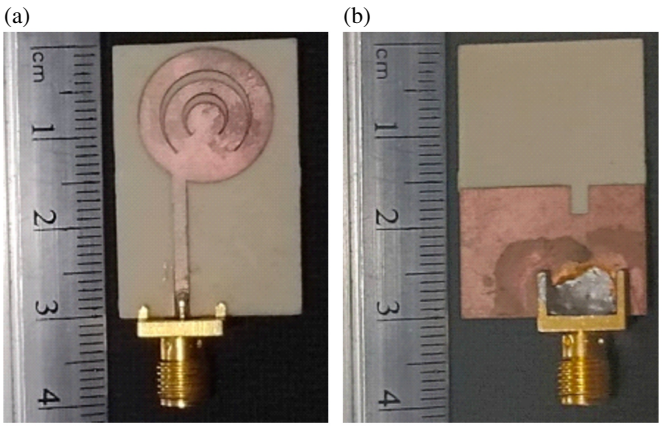

FIGURE 8. Photograph of the fabricated double crescent slots circular UWB circular monopole antenna. (a) Top view. (b) Bottom view.

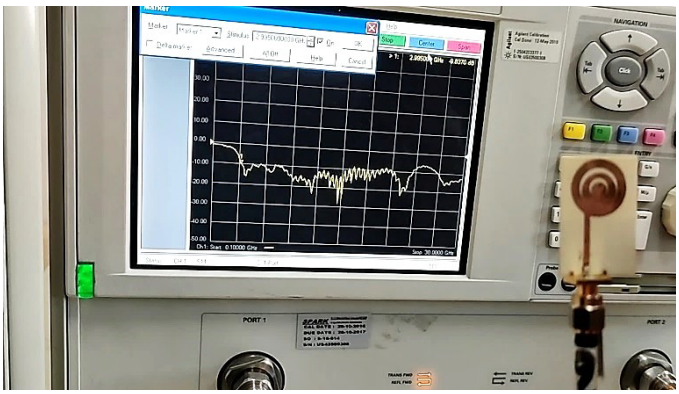

FIGURE 9. Measurement setup of the S_{11} parameter of the proposed antenna.

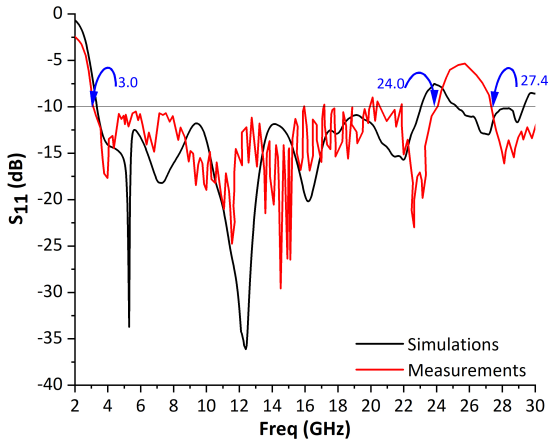

FIGURE 10. S_{11} parameter simulations and measurements of the proposed antenna.

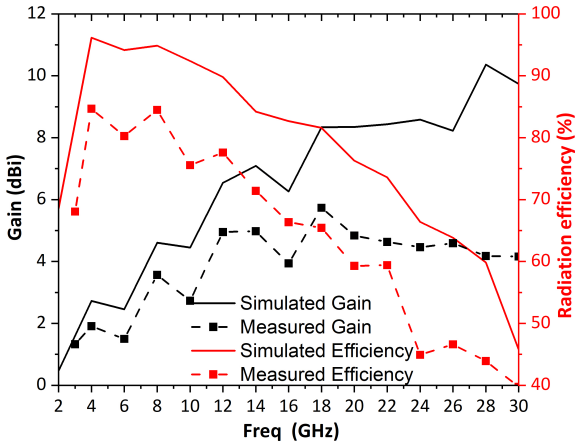

FIGURE 11. Simulated and measured gains and efficiencies of the proposed antenna.

exhibits a slight advantage, showing slightly higher peak gains in this narrow segment of the frequency band.

4. RESULTS AND DISCUSSION

A prototype of the proposed monopole antenna was fabricated on an FR4 substrate to validate the simulated performance. The fabricated antenna, as shown in Figure 8, maintains the same geometrical parameters as the optimized design.

The reflection coefficient (S_{11}) was measured using a vector network analyzer (VNA) as depicted in Figure 9. The reflection coefficient (S_{11}) was measured using an E8364B Vector Network Analyzer from Agilent Technologies, as shown in Figure 9. The measurement setup consisted of an antenna connected through an SMA connector to the VNA, ensuring proper calibration and minimizing the measurement uncertainty.

The measured S_{11} response confirmed the wideband behavior of the proposed antenna and remains generally consistent with the simulated results, supporting its suitability for UWB applications. The measured and simulated reflection coefficient (S_{11}) responses, as shown in Figure 10, were compared over the frequency range of 2–30 GHz. The design attains a measured impedance bandwidth extending from 3 GHz to 24 GHz, with an additional higher band 27.4–30 GHz. Both curves exhibit a similar overall trend, with prominent resonances at approximately 4 GHz, 11.5 GHz, 15 GHz, 23 GHz, and 28 GHz, indicating effective impedance matching at these frequencies. As expected, the simulated results present smoother and deeper resonances owing to idealized conditions, while the measured data show slightly shallower dips and additional fluctuations, particularly between 10 and 20 GHz. In the lower-frequency range, the measured response shows some deviation from the simulated curve, which is primarily attributed to practical measurement factors that are difficult to perfectly replicate in simulation, including fabrication tolerances, slight misalignment, the SMA connector, which was not included in the simulation model, and its soldering interface, manufacturing tolerances in the thickness of the substrate, dimensions of the slots, DGS, etc., in addition to environmental perturbations during testing, which may add extra ripples and slightly raise the measured S_{11}. Despite these deviations, the measured response still covered the intended operating band, and the overall behavior remained admissibly consistent with the simulation. The observed differences highlight practical factors that can be further reduced through

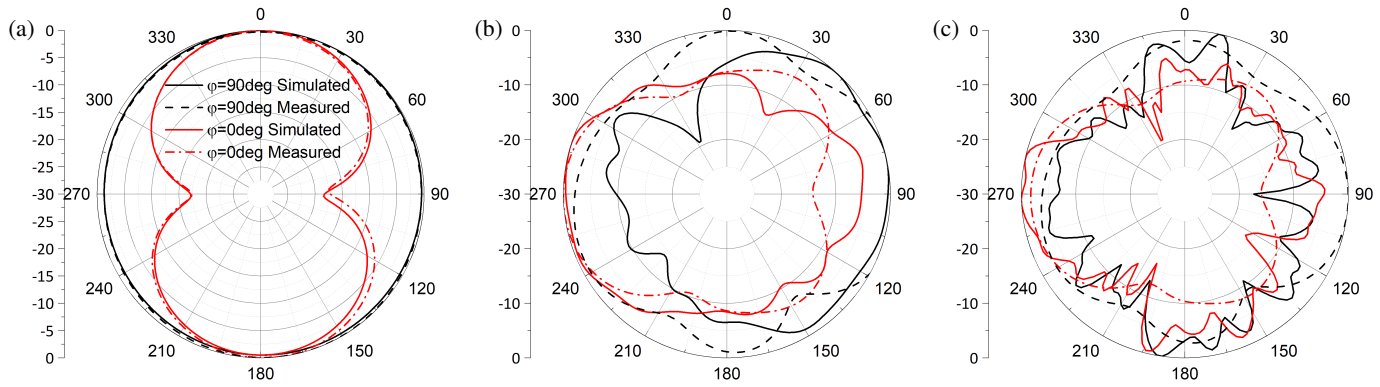

FIGURE 12. Normalized radiation pattern for the proposed antenna in different planes (XZ and YZ). (a) 3.1, (b) 10.5 and (c) 18 GHz.

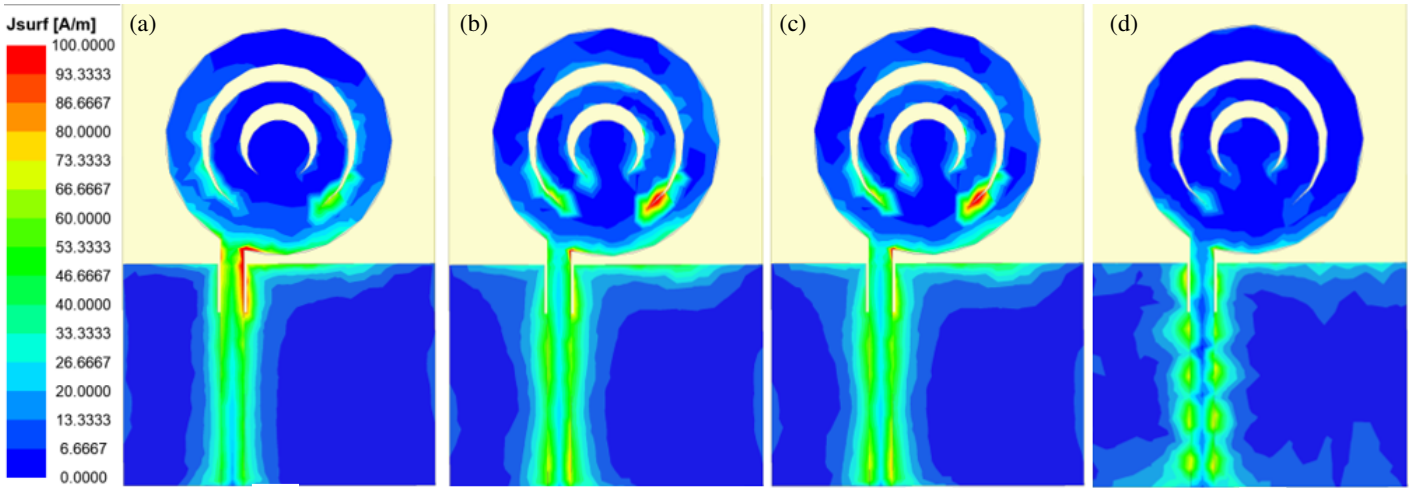

FIGURE 13. Complex magnitude of the current distribution at different frequencies. (a) 3.5, (b) 10.5, (c) 18, and (d) 28 GHz.

improved calibration, tighter fabrication control, and refined modeling techniques. Figures 11 and 12 depict the simulated and measured gains and efficiencies, and the normalized radiation patterns of the proposed antenna, respectively. The measurements were performed using a standard far-field setup inside an anechoic chamber. A Keysight PNA-L Vector Network Analyzer was employed to perform the radiation pattern, gain, and efficiency measurements using a classical transmission configuration, where the antenna under test was illuminated by a calibrated standard gain horn.

The results showed a clear and consistent trend across the entire frequency band. Both gain curves rise up to approximately 12 GHz, where the simulated gain reaches approximately 6.5–8 dBi, and the measured gain is approximately 5–6.6 dBi. Beyond this point, the gain remained relatively stable, with the simulated curve fluctuating between 7 and 10 dBi, whereas the measured values remained slightly lower. The simulated efficiency starts to be high, above 90% and gradually decreases to approximately 40% at 28 GHz, and the measured efficiency follows the same downward trend but with lower values. These differences were mainly caused by conductor and dielectric losses at higher frequencies, connector imperfections, and small impedance mismatches in the fabricated prototype. Overall, the close agreement between simulation and measurement validates the antenna design and confirms its reliable broadband performance.

Figure 13 shows the normalized simulated and measured radiation patterns of the proposed antenna in the E-plane ($\phi = 0°$) and H-planes ($\phi = 90°$) at 3.5, 10.5, and 18 GHz. At 3.5 GHz, the antenna exhibited an almost omnidirectional pattern, typical of a monopole mode, with excellent agreement between simulation and measurement, confirming the design's reliability. At 10.5 GHz, both patterns maintained a similar overall shape, with minor discrepancies in side-lobe levels and null positions, likely due to measurement uncertainties, connector effects, or reflections in the anechoic chamber. Despite these differences, the main beam direction remains consistent, indicating stable mid-band performance. At 18 GHz, the patterns became more complex because of higher-order mode excitation and the influence of the finite ground plane. The measured lobes appeared slightly broader or shifted, mainly because of the fabrication tolerances and feed misalignment at high frequencies. The antenna demonstrates good agreement between the simulation and measurement in the entire band, with acceptable variations typical of high-frequency operation.

TABLE 3. Comparison of the proposed antenna design with published studies.

Ref.	Substrate	Dimensions	Frequency band (GHz)	Gain range	Radiation efficiency range (%)
[10]	FR4	$26.8 \times 26 \times 1.575$	3.43–4.25, 6.57–7.81	2.1–3.5	75–85
[13]	Jeans	$46.3 \times 52.6 \times 1.076$	2.95–24.2	0–3.16	–
[14]	Denim	$31 \times 31 \times 0.7$	2–11.6	–	–
[16]	FR4	$40 \times 40 \times 1.6$	5.36–7.62	1–4.2	–
[18]	FR4	$30 \times 20 \times 1.6$	2–6	–	–
[20]	FR4	$30 \times 29 \times 1.6$	3.2–11.92	1.5–6.43	–
[24]	FR4	$46 \times 38 \times 1.6$	2.1–2.8, 5.6–6.5, 12.7–16	1–6	62–87
[27]	FR4	$40 \times 36 \times 1$	2.2–3.3, 4.3–5.1, 6.3–10.8	–	–
[30]	FR4	$50 \times 50 \times 1.6$	2.1–12.6	3.5–7	90–97
[38]	Duroid 5880	$30 \times 24 \times 0.787$	3–12.7	0.5–3.6	70–95
[39]	Denim	$60 \times 50 \times 0.7$	7–28	–	83–94
[49]	FR4	$40 \times 34 \times 1.6$	2.30–4.10, 6.10–10.0	2–9	60–92
[52]	FR4	$30 \times 32 \times 1.6$	3.01–3.75, 6.74–13.86	1.55–6.67	–
[53]	FR4	$32 \times 36 \times 1.6$	2.35–2.78, 3.46–4.65, 5.08–6.08, 7.96–13	–7.13	–
[55]	Duroid 5880	$55 \times 70 \times 1.57$	1.46–3.2	2.56–3.6	–
[64]	FR4	$35 \times 30 \times 1.6$	3.03–11.75	–	65–85
This work	FR4	$30 \times 20 \times 0.8$	3–24	1.3–6.6	45–86

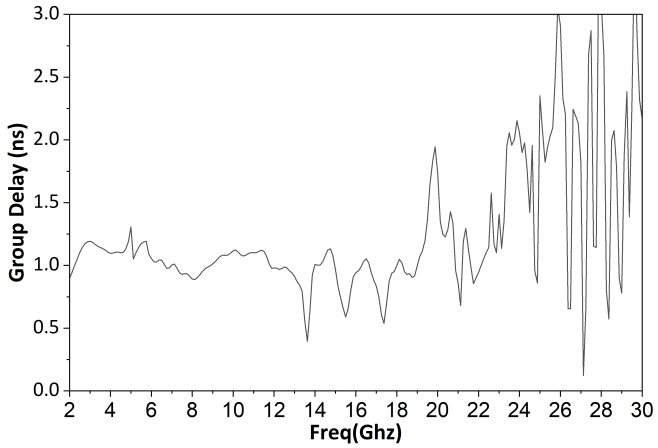

FIGURE 14. Simulated group delay of the proposed antenna.

Figure 13 shows the current distribution on the monopole antenna at 3.5 GHz, 10.5 GHz, 18 GHz, and 28 GHz. As the frequency increases from 3.5 GHz to 28 GHz, the current distribution on the monopole antenna shifts from a simple fundamental mode with a single peak near the feed to more complex higher-order modes featuring multiple peaks and nodes. This corresponds to an antenna supporting multiple resonant paths and standing wave patterns, which impact the radiation characteristics and antenna impedance [22]. The group delay of a UWB antenna is a critical parameter for evaluating its time-domain performance, as it directly indicates the extent of pulse distortion. A low and stable group delay (ideally constant across the operating bandwidth) is essential for preserving the shape of short-duration pulses, thereby ensuring high fidelity in applications requiring minimal dispersion, such as high-data-rate wireless communications, high-resolution radar, and body-centric imaging systems. The group delay is defined as the negative rate of change of the transfer function phase, $\phi(\omega)$ with respect to frequency. This can be calculated as follows [38, 63]:

$$\tau(\omega) = -\frac{d\phi(\omega)}{d\omega} \tag{1}$$

To evaluate the group delay, a two-antenna transmission setup was implemented in ANSYS HFSS, where identical antennas were placed in the far-field region to eliminate near-field coupling effects. For UWB applications, maintaining $|\tau| \leq 2$ ns is generally required to ensure good phase linearity and minimal signal distortion in the time domain [38]. Figure 14 shows that the group delay remains relatively flat within the 2–19 GHz range, with an average value of approximately 1 ns, indicating low dispersion and a nearly linear phase response suitable for wideband signal transmission. In the 19–24 GHz region, the group delay begins to increase and exhibits several resonant peaks reaching 2.0–2.4 ns. Beyond 24 GHz, a strong variation is observed, with values fluctuating between 0.1 ns and 3.6 ns and multiple spikes exceeding 3 ns, revealing significant dispersion that would introduce noticeable waveform distortion. The simulated group delay stays below 2 ns over the 2–23.5 GHz band, confirming that the antenna maintains acceptable time-domain behavior for broadband applications.

Table 3 presents a comparison of the proposed antenna with several designs reported in the literature. Most previous studies have used FR4 substrates, providing moderate bandwidth and efficiency. A few studies have explored fabric-based materials such as jeans and denim, which offered very wide fre-

quency coverage up to 28 GHz but suffered from larger size and lower gain because of higher material losses. For FR4-based designs, the operating frequencies generally ranged from 2 GHz to 12.7 GHz, and the peak gain rarely exceeds 10 dBi. The antennas reported in [20] and [30] achieved relatively high gains of 6.43 dBi and 9.8 dBi, respectively, but their operation bandwidths are still narrower, and their overall sizes remain larger than those of the present design. The proposed antenna stands out by combining a very wide band (3–24 GHz) with a compact size ($30 \times 20 \times 0.8\,\text{mm}^3$) smaller than most existing models. It also maintains a peak gain of 6.6 dBi and a radiation efficiency of 86%, indicating that the design efficiently radiates over a broad spectrum without significant performance loss. The proposed antenna achieves an excellent balance among miniaturization, bandwidth, and efficiency, making it a strong candidate for portable and biomedical applications, 5G, MBAN/WBAN, and Iot UWB applications.

5. CONCLUSION

A compact circular monopole antenna incorporating dual crescent-shaped slots and a defective ground structure was successfully designed, optimized using ANSYS HFSS, and experimentally validated for UWB applications. Through a systematic four-step evolution process, the effects of the feed offset, slot configuration, and ground-plane modification on impedance and radiation characteristics were thoroughly investigated. The final prototype achieved a measured -10 dB impedance bandwidth extending from 3 to 24 GHz, with an additional higher band up to 29 GHz, effectively covering multiple wireless and radar frequency ranges. The antenna exhibited a peak gain of 6.6 dBi, maintaining stable and nearly omnidirectional radiation at lower frequencies and more directive patterns at higher bands. The good agreement between the simulated and measured results confirms the reliability of the HFSS model and fabrication process. Owing to its compact size, wide impedance bandwidth, and versatile radiation performance, the proposed antenna is a strong candidate for 5G, IoT, radar, and biomedical imaging systems that require compact and broadband wireless front-ends.

ACKNOWLEDGEMENT

This study was funded by the European Union's Horizon Europe Research and Innovation Program under grant agreement HE-MSCA-SE-6G-TERAFIT101131501 and in part by the Direction Générale de la Recherche Scientifique et du Développement Technologique (DGRSDT), Ministry of Higher Education and Scientific Research (MESRS), Algeria. The funding information was not applicable because no funding was received.

REFERENCES

[1] Hammache, B., I. Messaoudene, M. Belazzoug, S. Titouni, A. Messai, and T. A. Denidni, "Gain enhancement of compact CPW-fed ultra-wideband antenna using an FSS reflector," *Microwave and Optical Technology Letters*, Vol. 66, No. 10, e34344, 2024.

[2] Park, S. and K.-Y. Jung, "Novel compact UWB planar monopole antenna using a ribbon-shaped slot," *IEEE Access*, Vol. 10, 61 951–61 959, 2022.

[3] Arora, S., S. Sharma, and R. Anand, "Ultra-wideband antenna with quintuple band notches integrated with metamaterials," *Progress In Electromagnetics Research M*, Vol. 122, 41–52, 2023.

[4] Essid, C., C. Abdelhamid, F. A. Almalki, O. Ali, and H. Sakli, "New MIMO antenna with filtration for the future multiuser systems in satellite communications," *Wireless Communications and Mobile Computing*, Vol. 2022, No. 1, 1040333, 2022.

[5] Koohestani, M. and Azadi-Tinat, N. and Skrivervik, A. K., "Compact slit-loaded ACS-fed monopole antenna for Bluetooth and UWB systems with WLAN band-stop capability," *IEEE Access*, Vol. 11, 7540–7550, 2023.

[6] Govindan, T., S. K. Palaniswamy, M. Kanagasabai, S. Kumar, M. Marey, and H. Mostafa, "Design and analysis of a flexible smart apparel MIMO antenna for bio-healthcare applications," *Micromachines*, Vol. 13, No. 11, 1919, 2022.

[7] Cha, S. G., Y. J. Yoon, Y. J. Lee, S. T. Hong, H. S. Mun, and Y. H. Park, "Integrated module antenna for automotive UWB application," *Applied Sciences*, Vol. 12, No. 22, 11423, 2022.

[8] Nahas, M., "A high-gain dual-band slotted microstrip patch antenna for 5G cellular mobile phones," *Engineering, Technology & Applied Science Research*, Vol. 14, No. 3, 14 504–14 508, 2024.

[9] Dey, R., M. K. Ray, and K. Mandal, "A low-profile circularly polarized patch antenna with wide axial ratio bandwidth," *Physica Scripta*, Vol. 100, No. 4, 045549, 2025.

[10] Paul, S., S. Rana, A. R. Azad, D. Nandi, and A. Mohan, "Compact planar UWB microstrip antenna with independently controllable dual notch bands," *ETRI Journal*, Vol. 47, No. 6, 1125–1138, 2025.

[11] Singh, C., C. Sharma, and A. Kumar, "Miniaturized Ultra-Wideband microstrip antenna with triple band-notched characteristics at WiMAX/WLAN/X-band for medical applications," *Physica Scripta*, Vol. 100, No. 5, 055523, 2025.

[12] Xiang, Z., Z. Wang, C. Li, and R. You, "Design of UWB monopole antenna with ring structure based on characteristic mode theory," *Progress In Electromagnetics Research C*, Vol. 158, 225–234, 2025.

[13] Singh, A., R. K. Dwivedi, V. K. Singh, M. Sharma, K. Sharma, and B. Yilmaz, "Modeling and simulation of an effectual triangular slotted UWB flexible antenna for breast cancer detection and healthcare monitoring," *PLoS ONE*, Vol. 20, No. 4, e0320806, 2025.

[14] Abdulla, F. A. a. and A. Demirkol, "A novel textile-based UWB patch antenna for breast cancer imaging," *Physical and Engineering Sciences in Medicine*, Vol. 47, No. 3, 851–861, 2024.

[15] Jujjuvarapu, J. K., A. Mareedu, P. V. G. Padamata, S. M. avuluri, and S. G. Nallari, "Design of microstrip fed patch antenna using DGS for UWB applications," *International Journal for Multidisciplinary Research*, Vol. 7, No. 2, 2025.

[16] Kodali, R. R., P. Siddaiah, and M. N. G. Prasad, "Bandwidth enhanced deltoid leaf fractal antenna for 5.8 GHz WLAN applications," *TELKOMNIKA (Telecommunication Computing Electronics and Control)*, Vol. 20, No. 5, 963–970, 2022.

[17] Çelik, K., "A novel circular fractal ring UWB monopole antenna with dual band-notched characteristics," *ETRI Journal*, Vol. 46, No. 2, 218–226, 2024.

[18] Abayaje, F., A. A. Alrawachy, and Y. S. Mezaal, "Design of compact UWB monopole patch antenna with octagonal shape for C-band, Wi-MAX, and WLAN applications," *Optoelectron-*

ics and Advanced Materials — Rapid Communications, Vol. 17, No. 7–8, 323–328, 2023.

[19] Sayad, D., C. Zebiri, H. Obeidat, I. Elfergani, A. Amroun, M. Palandoken, M. L. Bouknia, R. Zegadi, and J. Rodriguez, "New elliptical miniaturized antenna using concentric open rings for UWB applications," *Progress In Electromagnetics Research C*, Vol. 134, 79–91, 2023.

[20] kumar, N. N., B. S. Srikanth, S. B. Gurung, S. Manu, G. N. S. Gowthami, T. Ali, and S. Pathan, "A slotted UWB monopole antenna with truncated ground plane for breast cancer detection," *Alexandria Engineering Journal*, Vol. 59, No. 5, 3767–3780, 2020.

[21] Amroun, A., C. Zebiri, D. Sayad, I. T. E. Elfergani, A. Desai, M. L. Bouknia, R. Zegadi, and J. Rodriguez, "Miniaturized six-ring elliptical monopole-based MIMO antenna for ultrawideband applications," *International Journal of Communication Systems*, Vol. 36, No. 14, e5557, 2023.

[22] Ji, F., H. Zhang, X. Xing, W. Lu, and L. Zhu, "Dual-mode resonant sectorial monopole antenna with stable backfire gain," *Chinese Journal of Electronics*, Vol. 33, No. 6, 1478–1486, 2024.

[23] Singh, C. and C. Sharma, "A miniaturized SC-DGS tapered-fed notched uwb antenna designed for breast tumor detection applications," *Physica Scripta*, Vol. 100, No. 6, 065529, 2025.

[24] El-Hakim, H. A. and H. A. Mohamed, "Engineering planar antenna using geometry arrangements for wireless communications and satellite applications," *Scientific Reports*, Vol. 13, No. 1, 19196, 2023.

[25] Arora, S., S. Sharma, R. Anand, and G. Shrivastva, "Miniaturized pentagon-shaped planar monopole antenna for ultra-wideband applications," *Progress In Electromagnetics Research C*, Vol. 133, 195–208, 2023.

[26] Kumari, R. and V. K. Tomar, "A compact four-element electromagnetic band gap and slots-inspired ultra-wideband multiple-input-multiple-output antenna with quad-band rejection characteristics," *Advanced Electromagnetics*, Vol. 14, No. 2, 9–19, 2025.

[27] Du, Y. and M. Liu, "A dual-notched ultra-wideband monopole antenna based on frequency selective surface technology," *Progress In Electromagnetics Research C*, Vol. 145, 101–105, 2024.

[28] Bensid, C., M. L. Bouknia, D. Sayad, I. Elfergani, H. Bendjedi, R. Zegadi, J. Rodriguez, A. Varshney, and C. Zebiri, "A novel pentagonal-shaped monopole antenna with a CSRR metamaterial loaded defected ground for UWB applications," *Progress In Electromagnetics Research C*, Vol. 139, 175–185, 2024.

[29] Tighilt, Y., C. Bensid, D. Sayad, S. Mekki, R. Zegadi, M. L. Bouknia, I. Elfergani, P. Singh, J. Rodriguez, and C. Zebiri, "Low-profile UWB-MIMO antenna system with enhanced isolation using parasitic elements and metamaterial integration," *Electronics*, Vol. 12, No. 23, 4852, 2023.

[30] Al-Gburi, A. J. A., I. B. M. Ibrahim, Z. Zakaria, B. H. Ahmad, N. A. B. Shairi, and M. Y. Zeain, "High gain of UWB planar antenna utilising FSS reflector for UWB applications," *Computers, Materials & Continua*, Vol. 70, No. 1, 1419–1436, 2022.

[31] Merin Joshiba, J. and D. Judson, "An eye bolt shape slotted microstrip patch antenna design utilizing a substrate-integrated waveguide for 5G systems," *Automatika*, Vol. 64, No. 4, 943–955, 2023.

[32] Mohamadzade, B., R. B. V. B. Simorangkir, R. M. Hashmi, and A. Lalbakhsh, "A conformal ultrawideband antenna with monopole-like radiation patterns," *IEEE Transactions on Antennas and Propagation*, Vol. 68, No. 8, 6383–6388, 2020.

[33] Izuddin, N. Y. bt N., O. bin Ayop, and F. bin Zubir, "A comparative study of four defected ground structures for ultra-wideband planar antenna application at 3.5 GHz," *ELEKTRIKA — Journal of Electrical Engineering*, Vol. 24, No. 2, 98–103, 2025.

[34] Subhash, B. K. and R. C. Biradar, "A rectangular slotted dual-notch UWB antenna for wireless communication application," *Telecommunications and Radio Engineering*, Vol. 83, No. 2, 27–36, 2024.

[35] Addepalli, T., V. Prakasam, M. S. Kumar, P. R. Sura, A. L. Siridhara, M. Venkatanaresh, R. Uppada, and A. L. Narayana, "Triple band notched UWB antenna for short distance high speed wireless communication systems," *Telecommunications and Radio Engineering*, Vol. 84, No. 9, 19–38, 2025.

[36] Rao, P. S., M. V. S. Prasad, and V. R. S. Redy, "Triple band-notched UWB planar monopole antenna using circular slots," *Telecommunications and Radio Engineering*, Vol. 83, No. 10, 29–42, 2024.

[37] Nawati, V. R., B. K. Sujatha, G. S. Karthikeya, A. Desai, H. T. Hsu, and M. Palandoken, "A compact dual-polarized probe-fed UWB antenna system for breast cancer detection applications," *Wireless Networks*, Vol. 30, No. 5, 3039–3050, 2024.

[38] Khan, M. A., U. Rafique, H. □. Savci, A. N. Nordin, S. H. Kiani, and S. M. Abbas, "Ultra-wideband pentagonal fractal antenna with stable radiation characteristics for microwave imaging applications," *Electronics*, Vol. 11, No. 13, 2061, 2022.

[39] Mahmood, S. N., A. J. Ishak, T. Saeidi, A. C. Soh, A. Jalal, M. A. Imran, and Q. H. Abbasi, "Full ground ultra-wideband wearable textile antenna for breast cancer and wireless body area network applications," *Micromachines*, Vol. 12, No. 3, 322, 2021.

[40] Din, I. U., S. Ullah, S. I. Naqvi, R. Ullah, S. Ullah, E. M. Ali, and M. Alibakhshikenari, "Improvement in the gain of uwb antenna for GPR applications by using frequency-selective surface," *International Journal of Antennas and Propagation*, Vol. 2022, No. 1, 2002552, 2022.

[41] Saeed, M. J., M. M. Tahseen, and A. A. Kishk, "Compact multi-band omni-directional antenna for maximizing frequency coverage," *IEEE Antennas and Wireless Propagation Letters*, Vol. 24, No. 3, 597–601, 2025.

[42] Fakharian, M. M., "A compact UWB antenna with dynamically switchable band-notched characteristic using broadband rectenna and DC-DC booster," *International Journal of Microwave and Wireless Technologies*, Vol. 13, No. 10, 1086–1095, 2021.

[43] Abayaje, F., Y. S. Mezaal, and B. M. Alameri, "UWB monopole patch antenna with two H-shaped slots and dual-band notch for WLAN and WiMAX applications," in *Proceedings of the Estonian Academy of Sciences*, Vol. 70, No. 2, 148–154, 2021.

[44] Rakluea, P., N. Wongsin, C. Mahatthanajatuphat, P. Aroonmitr, T. Jangjing, C. Rakluea, W. Chanwattanapong, and N. Chudpooti, "Flexible thin film-based triple port UWB MIMO antenna with modified ground plane for UWB, WLAN, WiMAX, WPAN and 5G applications," *IEEE Access*, Vol. 11, 107 031–107 048, 2023.

[45] Parida, R. K., A. K. Sahu, D. K. Naik, P. Raiguru, D. C. Panda, and R. K. Mishra, "Compact reconfigurable antenna system for spectrum interweaved cognitive radio," *International Journal of RF and Microwave Computer-Aided Engineering*, Vol. 32, No. 7, e23183, 2022.

[46] Pandey, U., P. Singh, R. Singh, N. P. Gupta, S. K. Arora, and E. Nizeyimana, "Miniaturized ultrawideband microstrip antenna for IoT-based wireless body area network applications," *Wireless Communications and Mobile Computing*, Vol. 2023, No. 1, 3950769, 2023.

[47] Lamultree, S., M. Phalla, P. Kunkritthanachai, and C. Phongcharoenpanich, "Design of a circular patch antenna with parasitic elements for 5G applications," *International Journal of Engineering*, Vol. 36, No. 9, 1686–1694, 2023.

[48] Mishra, P. K., T. K. Patnaik, B. P. Panda, and R. K. Mishra, "A compact high gain uwb planar monopole antenna using circular slots," *Serbian Journal of Electrical Engineering*, Vol. 21, No. 2, 201–216, 2024.

[49] Marzouk, M., Y. Rhazi, I. H. Nejdi, F.-E. Zerrad, M. Saih, S. Ahmad, A. Ghaffar, and M. Hussein, "Ultra-wideband compact fractal antenna for WiMAX, WLAN, C and X band applications," *Sensors*, Vol. 23, No. 9, 4254, 2023.

[50] Kim, G. and S. Kim, "Design and analysis of dual polarized broadband microstrip patch antenna for 5G mmWave antenna module on FR4 substrate," *IEEE Access*, Vol. 9, 64 306–64 316, 2021.

[51] Hamad, E. K. I. and G. Nady, "Bandwidth extension of ultra-wideband microstrip antenna using metamaterial double-side planar periodic geometry," *Radioengineering*, Vol. 28, No. 1, 25–32, 2019.

[52] Ketavath, K. N., "Dual-band crescent-shaped slot patch antenna for wireless communications and IoT applications," *Microwave and Optical Technology Letters*, Vol. 65, No. 8, 2392–2398, 2023.

[53] Thakur, S., R. Mishra, S. K. Soni, and P. K. Rao, "Crescent shaped slot loaded antenna sensor with tri-band notched for cancer detection," *Frequenz*, Vol. 76, No. 9-10, 569–578, 2022.

[54] Giri, K. K., R. K. Singh, and K. Mamta, "Effect of symmetric shaped slot on patch antenna design and performance for 10 GHz 5G applications," *Journal of Scientific Research*, Vol. 14, No. 2, 405–417, 2022.

[55] Asmeida, A., Z. Z. Abidin, S. M. Shah, M. R. Kamarudin, N. A. Malek, and J. Nebhen, "Wideband crescent-shaped slotted printed antenna with radiant circular polarisation," *International Journal of Antennas and Propagation*, Vol. 2021, No. 1, 9975679, 2021.

[56] Mutashar, R. A., A. S. Tahir, and W. A. G. Al-Tumah, "Design of high gain slotted circular microstrip antenna for X-band applications," *Basrah Journal of Sciences*, Vol. 39, No. 3, 414–431, 2021.

[57] Krishnan, T., S. Sennan, V. Ravi, and D. H. reddy, "A dual-band circular patch antenna using hexagon-shaped slots," *International Journal of Communication Systems*, Vol. 35, No. 9, e5125, 2022.

[58] Raj, T., R. Mishra, P. Kumar, and A. Kapoor, "Advances in MIMO antenna design for 5G: A comprehensive review," *Sensors*, Vol. 23, No. 14, 6329, 2023.

[59] Ramya, C. M. and R. B. Rani, "A circular triangle fractal antenna for high gain UWB communications with band rejection capability," *Progress In Electromagnetics Research M*, Vol. 110, 83–96, 2022.

[60] Guo, L., M. Min, W. Che, and W. Yang, "A novel miniaturized planar ultra-wideband antenna," *IEEE Access*, Vol. 7, 2769–2773, 2018.

[61] Vyas, K. and R. P. Yadav, "Planar suspended line technique based UWB-MIMO antenna having dual-band notching characteristics," *International Journal of Microwave and Wireless Technologies*, Vol. 13, No. 6, 614–623, 2021.

[62] Fakharian, M. M., "A wideband fractal planar monopole antenna with a thin slot on radiating stub for radio frequency energy harvesting applications," *Transactions B: Applications*, 2181–2187, 2020.

[63] Chen, B., Z. Li, Z. Xu, J. Wan, Z. Li, Y. Xiong, and Y. Pu, "Ultra-wideband high gain low group delay variation amplifier for phased-array radar system," *Microelectronics Journal*, Vol. 146, 106157, 2024.

[64] Xiang, Z., Z. Wang, C. Li, and R. You, "Design of UWB monopole antenna with ring structure based on characteristic mode theory," *Progress In Electromagnetics Research C*, Vol. 158, 225–234, 2025.